

Fracture Nucleation Phenomena and Thermally Activated Crack Dynamics in Monocrystals

Leonardo Golubović¹ & Dorel Moldovan²

¹ Physics and Astronomy Department, West Virginia University, Morgantown, WV 26506-6315, USA

² Department of Mechanical and Industrial Engineering, Louisiana State University, Baton Rouge, LA 70803

Correspondence: Leonardo Golubović, Physics and Astronomy Department, West Virginia University, Morgantown, WV 26506-6315, USA. E-mail: lgolubov@wvu.edu

Received: July 9, 2020

Accepted: September 29, 2020

Online Published: June 30, 2021

doi:10.5539/apr.v13n1p42

URL: <http://dx.doi.org/10.5539/apr.v13n1p42>

Abstract

We explore irreversible thermally activated growth of cracks which are shorter than the Griffith length. Such a growth was anticipated in several studies [Golubović, L. & Feng, S., (1991). Rate of microcrack nucleation, *Physical Review A* 43, 5223. Golubović, L. & Peredera, A., (1995). Mechanism of time-delayed fractures, *Physical Review E* 51, 2799]. We explore this thermally activated growth by means of atomistic Monte-Carlo dynamics simulations of stressed monocrystals. This crack growth is stepwise. Each step is marked by nucleation of a microcavity close to the crack tip, and by creation of a passage connecting the microcavity and the crack. If the external tensile stress is weak, many such nucleation events occur before the crack length reaches the Griffith size. In addition to the simulations, we also present an analytic theory of the stepwise thermally activated crack growth. The theory explains surprising observation from our simulations that the thermally activated crack growth remains fairly well directed in spite of the stochastic nature of the crack growth process.

Keywords: Crack dynamics, Fracture nucleation phenomena, Atomistic dynamics

1. Introduction

Solids under external tensile stresses are examples of metastable states of matter similar to supercooled liquids or magnetic systems [Lifshits & Pitaevski, 1981]. The threshold of fast (“instantaneous”) failure is in fact a metastability limit, i.e., spinodal point. At this point, the external stress σ as a function of the strain reaches its maximum, σ_{max} . However, stressed solids can break under stresses that are significantly weaker than σ_{max} . It may however take a long time before weakly stressed solids break. That is, the fracture is time-delayed with relatively long life time which is a function of temperature and the applied stress [Brenner, 1965]. Time delayed fracture is physically related to the phenomena of micro-failure nucleation and growth [Golubović & Feng, 1991; Golubović & Peredera, 1995]. These phenomena are similar to nucleation phenomena in metastable states of matter [Lifshits & Pitaevski, 1981]. The classical work of Griffith (1921) contains some elements suggesting a phenomenological theory of microcrack nucleation. The critical, Griffith crack is somewhat similar to critical nucleus in a metastable state: Cracks longer than the Griffith crack rapidly and irreversibly grow [Mott, 1948]. The growth of cracks shorter than the Griffith crack size may seem unlikely due to energy reasons. Yet, such a growth still does occur in realistic systems due to thermally activated processes of failure nucleation [Brenner,

1965]. Recent examples of these phenomena are time-delayed fractures in stressed mechanical structures such as space elevators [Edwards & Westling, 2003; Golubović & Knudsen, 2009; Knudsen & Golubović, 2014; Golubović & Knudsen, 2019].

In the present study, we explore these thermally activated growth phenomena by means of atomistic Monte-Carlo dynamics simulations of stressed monocrystals. This growth is a sequence of steps each involving a nucleation of a microcavity in the crack tip region and creation of a passage between the microcavity and the crack. In the presence of weak external stresses, many such growth steps occur before the crack length reaches the Griffith size. In addition to the simulations, we also discuss an analytic theory of these phenomena. The theory elucidates the step-wise character of the thermally activated crack growth. The theory explains surprising fact that thermally activated crack growth remains fairly well directed in spite of the random nature of the growth process.

To elucidate the results of the present study, it will be needed to first review earlier theories of failure nucleation phenomena in solids under external tensile stresses. First attempt in this direction is inspired by early work of Griffith (1921); see also Landau & Lifshits (1970). In this so called classical theory of failure nucleation, microcracks are analogs of the stable phase droplets in a metastable state. Consider a micro-crack of length L in a solid under a uniaxial stress σ perpendicular to the crack in a 2d-solid. Its creation costs the energy

$$E(L) = gL - \frac{\sigma^2 L^2}{2Y} \quad , \quad (1)$$

where first term is the energy price of creating crack's edges [In Eq. (1), and in the following, we suppress various numerical factors of order unity.] Here, ga , with a the atomic size, is comparable to the binding energy of an atomic bond. Due to the crack opening its two edges separate by the distance $d = \sigma L/Y$; here $Y =$ Young modulus. This process partially diminishes the stress in a domain with area L^2 around the crack. This decreases solid's elastic energy by an amount $\approx L^2 \sigma^2 / 2Y$, i.e., the second term in Eq. (1). Crack energy Eq. (1) reaches its maximum at the crack length L value equal to the critical Griffith length,

$$L_G = \frac{gY}{\sigma^2} \quad ,$$

at which the crack creation energy Eq. (1) is of the order $E_G = E(L_G) = g^2 Y / \sigma^2$. Therefore, the Griffith length crack is unstable: For $L > L_G$, this instability eventually produces the familiar fast crack growth [Mott, 1948]. For $L < L_G$, one has $\frac{dE}{dL} > 0$ so the crack growth is disfavored. This situation is similar to that encountered in more common nucleation phenomena [Lifshits & Pitaevski, 1981]. The E_G seems to play the role of a nucleation energy barrier E_b . This analogy suggests the use of the standard Arrhenius law $R_N \sim \frac{1}{t_N} \sim \exp(-\frac{E_b}{k_B T})$, with $E_b =$

$E_G = \frac{g^2 Y}{\sigma^2}$, to evaluate the nucleation rate R_N - or the time t_N needed for the failure to be thermally nucleated.

Validity of this classical failure theory (based on Griffith size crack) is however not assured. This was emphasized by Golubović & Feng (1991, GF in the following). For example, surface diffusion [Herring, 1950a] may affect the morphology of crack edges and this may prevent closing of microcracks shorter than the Griffith length L_G . Such surface processes are significant only if the crack opening displacement $d = \sigma L/Y$ is greater than the atomic size a . This is the case for $L > L_{min}$ where L_{min} is the *minimal crack size* introduced in GF,

$$L_{min} = aY/\sigma \quad .$$

Since $g \approx aY$,

$$L_{min} = g/\sigma.$$

In view of the above arguments, GF suggested that the actual energy barrier for the fracture nucleation can be estimated as $E(L_{min})$, that is,

$$E_b = E(L_{min}) = gL_{min} = g^2/\sigma.$$

Thus,

$$E_G/E(L_{min}) \approx L_G/L_{min} \approx Y/\sigma \approx \sigma_{max}/\sigma.$$

Therefore, the failure nucleation rate in GF picture is, for weak stresses, $\sigma \ll \sigma_{max}$, substantially greater than that predicted in the classical theory based on critical Griffith size crack. Golubović & Peredera (1995, GP in the following) used atomistic dynamics simulation to readdress the problem of failure nucleation in solids. These simulations strongly indicate that *microcavities* rather than microcracks are major nucleated defects in the delayed fracture regime. Energy cost of a microcavity nucleation is very different in the physical character from the energy cost of the Griffith crack nucleation. In a 2d solid, with a cavity with linear size R , the energy cost of cavity creation is of the form,

$$E_{cav}(R) = gR - \sigma R^2, \quad (2)$$

where the first term is the cavity surface energy ($\sim R$ in 2d). In addition, the cavity energy in Eq. (2) also contains a cavity volume contribution ($\sim R^2$ in 2d) produced by the applied stress [GP; Herring, 1950b]. Indeed, the creation of the cavity causes an elongation of the solid along the direction of the externally applied stress. This causes a decrease the solid sample energy by an amount $\sim \text{stress} \times \text{cavity volume} \sim \sigma R^2$. By Eq. (2), cavity energy is at maximum at a critical cavity size which is of the order,

$$R_c = g/\sigma,$$

while the energy barrier E_b for the cavity nucleation is of the order,

$$E_b = E_{cav}(R_c) = gR_c = g^2/\sigma.$$

Notably, the above energy-barrier scale for failure nucleation, proposed in GP, coincides with the aforementioned energy barrier proposed (on different grounds) in GF. Likewise, the minimal crack length L_{min} introduced by GF coincides with the critical cavity size, R_c ,

$$R_c = L_{min},$$

In the following we will show that these length and energy scales enter a comprehensive picture of thermally activated crack growth. An early attempt to microscopically explore this growth was done long ago by Golubović and Moldovan (1995, GM in the following) in a short conference publication.

2. Atomistic dynamics simulations of thermally activated crack growth

Earlier studies discussed in the Introduction support the idea of thermally activated growth of cracks with lengths L in the range $L_G > L > L_{min}$. To elucidate the character of this growth, we employ atomistic (off lattice) Monte-Carlo dynamics simulations, technically similar to the simulations in GP and Golubović, Peredera & Golubović (1995).

Monte-Carlo dynamics is a close relative of overdamped Langevin dynamics. Such computational approaches are well suited for studying slow physical processes such as nucleation phenomena dominated by potential energy of particles. The use of Langevin style approaches allows for large time steps and thus enables simulating particle systems up to very long times.

We note that, relative to the aforementioned GM study, our present study features simulations done with systems which are run to significantly longer times. This feature is especially significant for the present study addressing very slow nucleation phenomena occurring in the regime of time delayed fractures. By virtue of having large time steps one can simulate and explore larger particle systems. This adds a significant element of realism to the results of Langevin style simulations of physical systems.

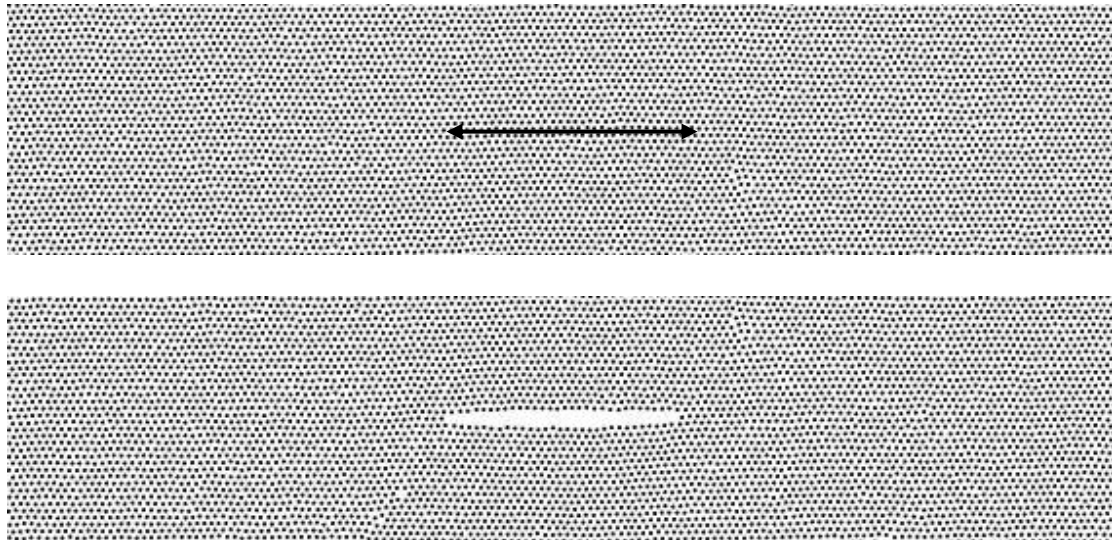


Figure 1: Preparation of the sharp (elastic) crack used in our simulations as the initial (preexisting) flaw: We start from a stressed sample without a crack. We switch off atomic interactions across a portion of a crystalline plane. The crack subsequently elastically opens. After that we restore the interactions.

In this study, we simulate behavior of cracks shorter than the Griffith length, $L < L_G$ in a 2d Lenard-Jones solid sample. In Figures 1 to 7 we give the time evolution of a solid sample initially containing such a crack. The sample is under an external tensile force $f = 225$ (in units for which the standard parameters of L-J potential are unity, i.e., $\sigma_{LJ} = 1$ and $\varepsilon_{LJ} = 1$) acting along the vertical direction. In Figures 1 to 7 we give only the middle portion of a larger sample with $12150 = 150 \times 81$ atoms at relatively low temperature which is twice smaller than the melting temperature.

Our goal here is to simulate the evolution of an artificially created flaw having the form of a *cut*. We are motivated by realistic experimental and practical situations in which one follows evolutions of preexisting flaws. *Initially sharp* (elastic) crack was prepared from a stressed sample without the crack by switching off interatomic interactions across a portion of the length L_0 of a horizontal crystalline plane [see Figure 1]. After the crack opening, we restored the interactions. If L_0 is smaller than $\approx 10a$, the restored attractive interactions quickly close the crack (leaving, sometimes, behind a few vacancies). If L_0 is longer than $\approx 60a$, the crack immediately proceeds to grow in a rapid fashion without any significant time delay. Hereafter, we present our results for the most interesting case when the initial crack size L_0 (here $= 32a$) is in the range $10a < L_0 < 60a$. In this range the crack growth is slowed down by the time delays related to nucleation processes underlying the crack growth. Figures 2 to 7 well illustrate these time delays in this slow crack growth. The time unit employed in Figures 2 to 7 is one Monte-Carlo Cycle (MCC). It involves updates of all particles' coordinates via Metropolis Monte-Carlo algorithm.

The most significant feature visible in Figures 2 to 7 is a notable nucleation of microcavities in the vicinity of the crack tips. This process goes on in a way similar to the one found in GP in the absence of an initially present (preexisting) crack. Here, however, the presence of the crack and consequent higher stress concentration at its tips strongly enhances the rate of microcavity nucleation and speeds up the subsequent sample failure that happens after about 140,000 MCC, see Figure 7.

For comparison, our simulations of the same sample *without* a preexisting crack indicate that the integrity of the sample is essentially intact, with only a few cavities, up to time-scales longer than one million MCC.

Slow crack growth in Figures 2 to 7 is a combination of the two basic types of processes: (i) nucleation of a microcavity close to a crack tip, followed by (ii) creation of a passage connecting the cavity with the crack tip. For example, in the vicinity of the right tip, a cavity was nucleated between 48,000 and 52,000 MCC [see Figures 3 and 4]. Subsequently, this microcavity was connected to the crack by a passage nucleated between 56,000 and 68,000 MCC [see Figure 4]. The further crack growth is dominated by a repeat of the same sequence of cavity nucleation followed by passage formation [see, for example, the events at the right crack tip between 80,000 and 88,000 MCC, Figure 5, and further crack evolution in Figures 6 and 7].

Manifestly, the time Δt needed to complete a cavity-passage creation cycle *decreases* as the crack size increases. For example, $\Delta t \approx 20,000$ MCC for the cavities in Figure 4, whereas $\Delta t \approx 8,000$ MCC for the cavities in Figure 5. Another notable feature in Figures 2 to 7 is that the size of the nucleated cavities also typically *decreases* as the crack size increases.

We discuss these growth features in Section 3. The overall crack growth is thus a sequence of steps each involving a cavity nucleation. This is manifest also in the shape of the crack surfaces that appears after many such steps, see Figures 6 and 7. We sketch this shape also in Figure 8 for the purposes of the discussions in Section 3.

Our simulations indicate that the creation of microcavities (vacancy clusters) is assisted by dislocations emitted by the crack tip which round (blunt) sharp crack tips. Interestingly, emitted dislocations frequently create bound states of a dislocation with a vacancy. These bound states decay by releasing a free dislocation. For example, at 20,000 MCC (Figure 2) we see such a dislocation-vacancy pair next to the left crack tip. Between 20,000 and 24,000 MCC a dislocation was released from the pair and started to glide in the upleft direction. Strikingly, during its gliding, this dislocation produces new vacancies. At 24,000 MCC we can see two such vacancies left behind the dislocation along its glide plane [one of them is close to the left crack tip, and soon gets connected to the mother crack by a passage nucleated between 28,000 and 32,000 MCC, see Figures 2 and 3]. As another example, the cavity close to the right crack tip at 52,000 MCC (Figure 4) was also produced during a glide of a dislocation which was initially next to this tip (see Figure 3 at 48,000 MCC). After assisting creation of the cavity we see near the right tip at 52,000 MCC, this dislocation continues to glide in the down-right direction, and, at about 56,000 MCC, it transforms into a dislocation-vacancy pair, a "fat dislocation" (see Figure 4 at 56,000 MCC). This pair is unstable and the dislocation is released, so that at 60,000 MCC we can see only a vacancy at its place. Apparently, dislocation emissions from crack tips play a fundamental role in the nucleation of vacancies and microcavities (vacancy clusters) in the vicinity of the crack tips. In addition, dislocation emissions produce plastic deformations rounding, i.e., blunting crack tips.

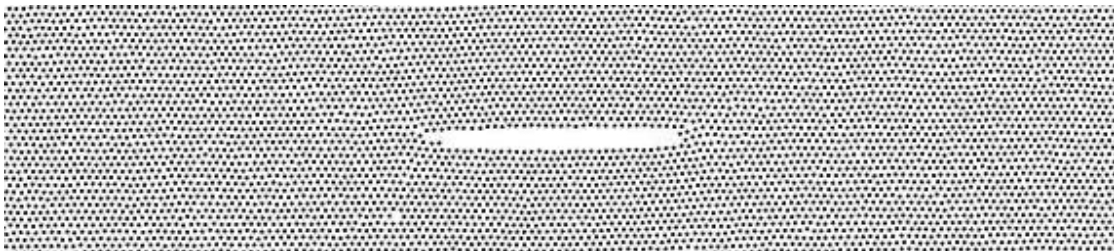
Our simulations thus evidence that thermally activated crack growth in monocrystals can go as a sequence of several different kinds of phenomena going on in the vicinity of the crack tip: (a) crack tip emits dislocations, (b) these dislocations then assist the creation of microcavities in the vicinity of the crack tip, and (c) passages

connecting the microcavities and the crack tips are formed. These successive phenomena cause increments of the crack length.

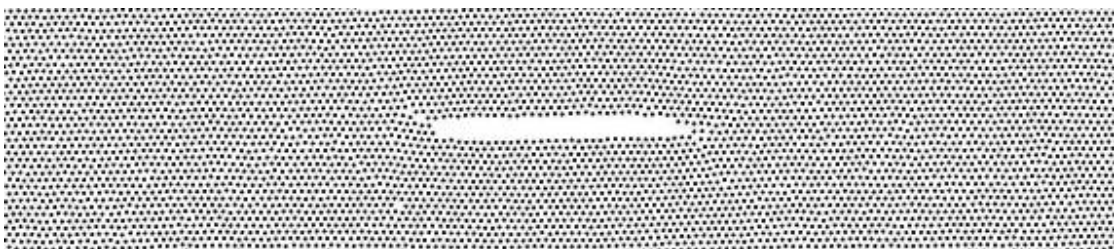
$t = 6000$



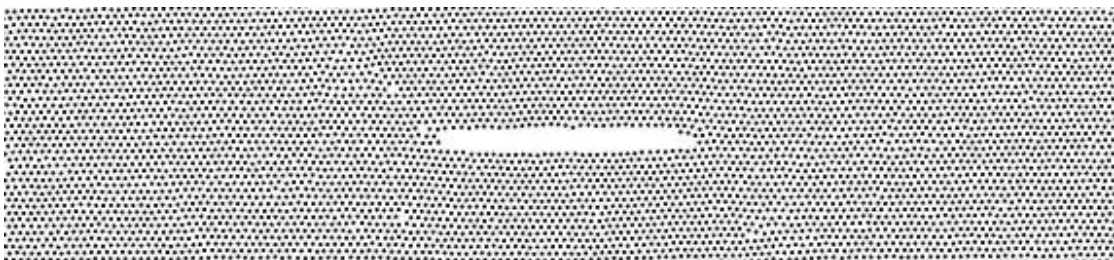
$t = 16000$



$t = 20000$



$t = 24000$



$t = 28000$

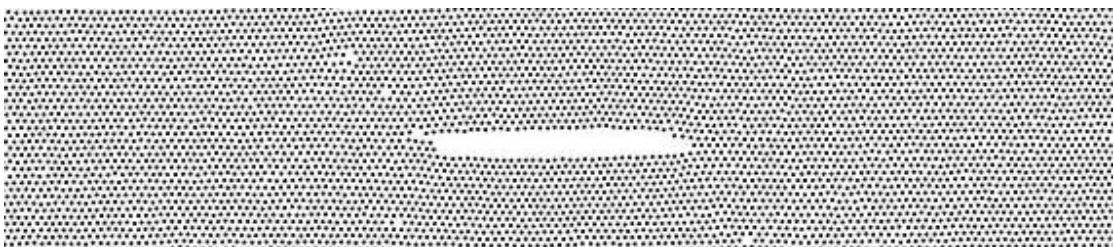
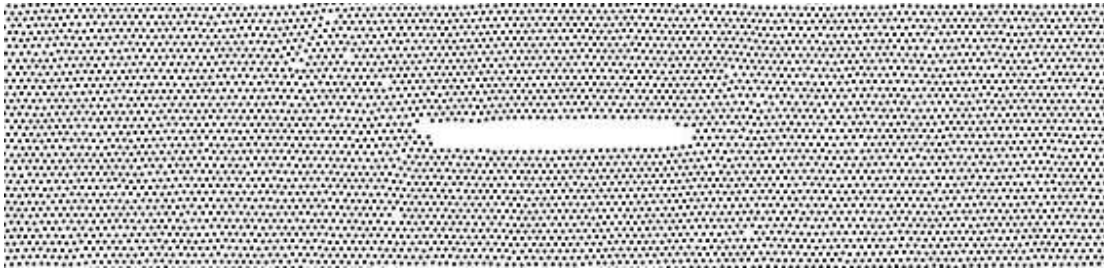
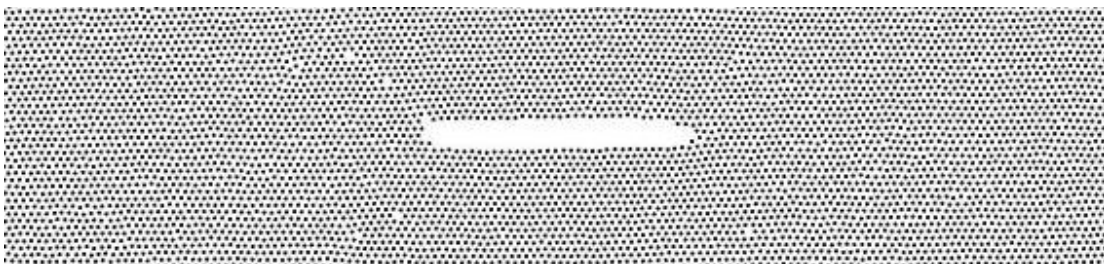


Figure 2: Crack dynamics between 6,000 and 28,000 MCC.

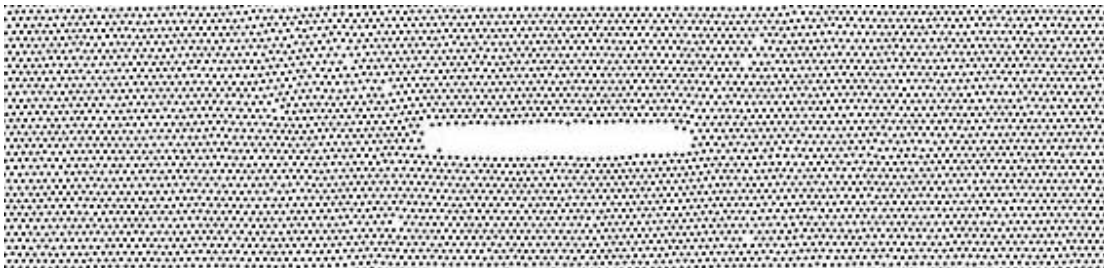
t = 32000



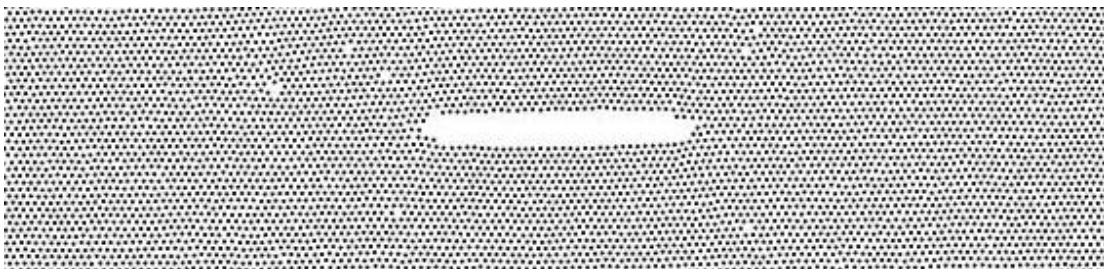
t = 36000



t = 40000



t = 44000



t = 48000

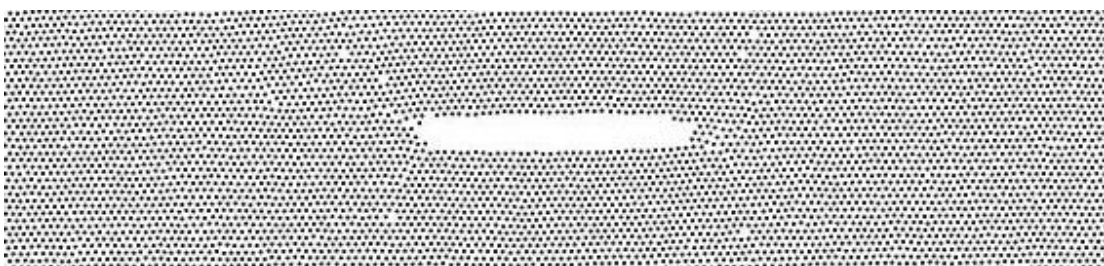
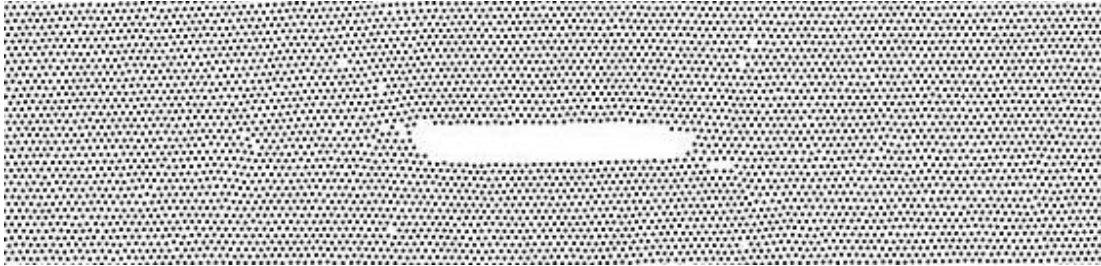
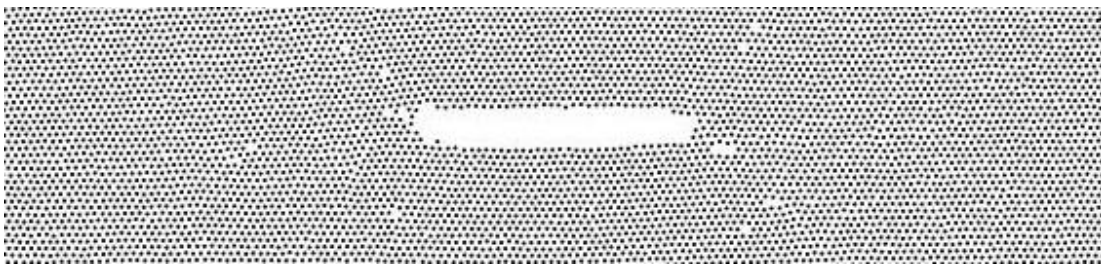


Figure 3: Crack dynamics between 32,000 and 48,000 MCC.

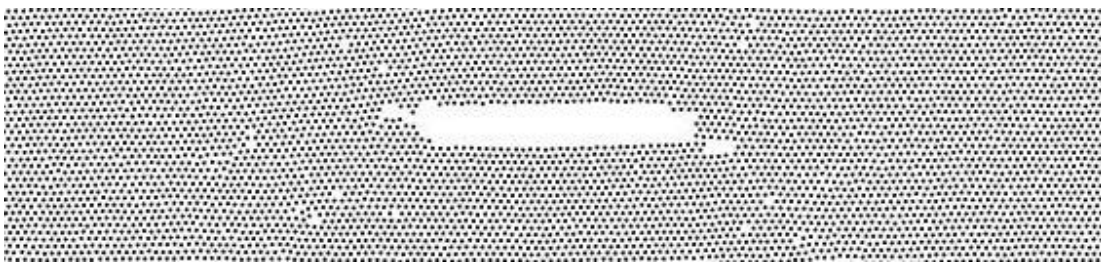
$t = 52000$



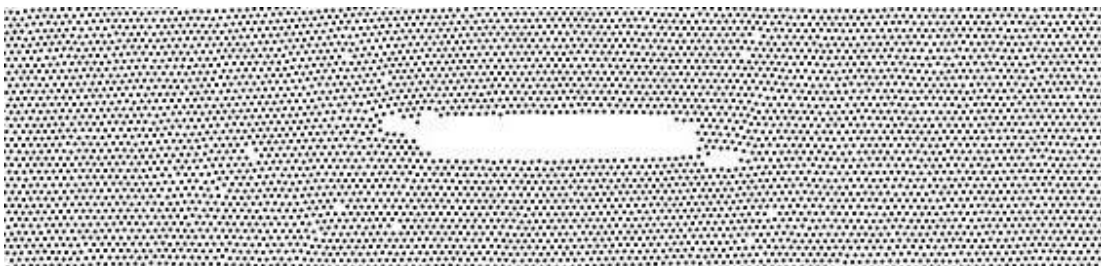
$t = 56000$



$t = 60000$



$t = 64000$



$t = 68000$

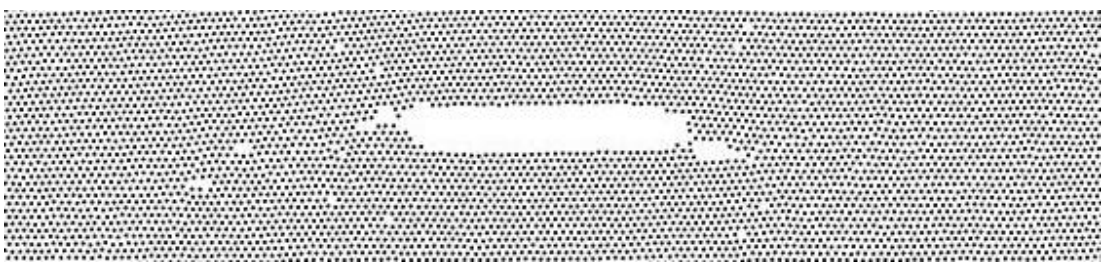
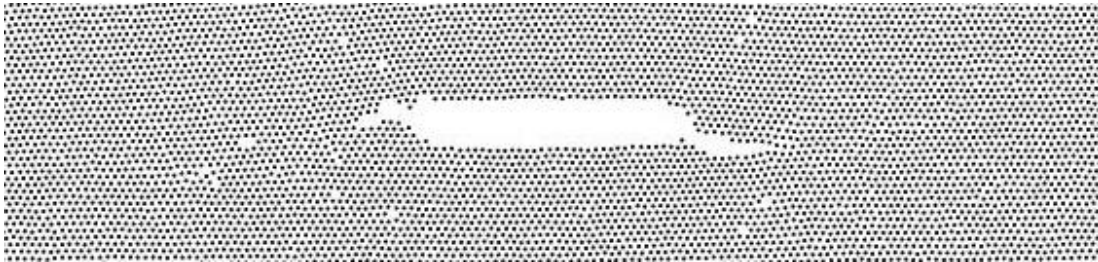
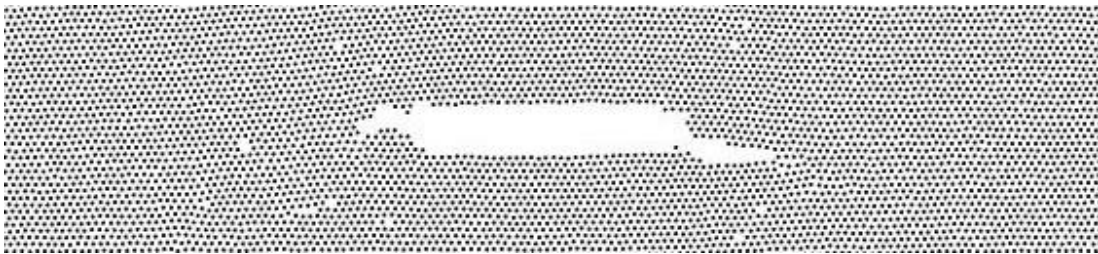


Figure 4: Crack dynamics between 52,000 and 68,000 MCC.

$t = 72000$



$t = 76000$



$t = 80000$



$t = 84000$



$t = 88000$

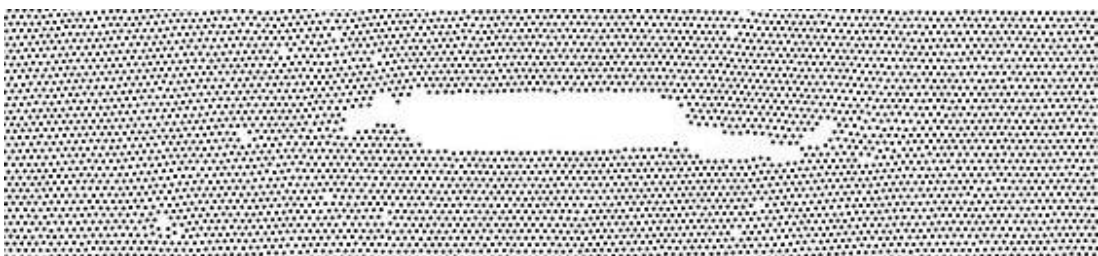
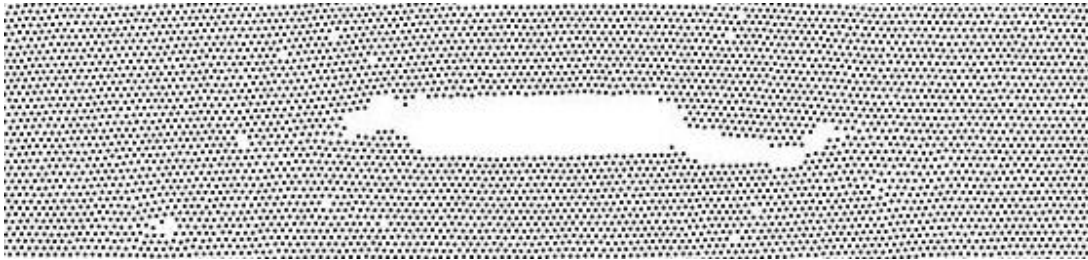
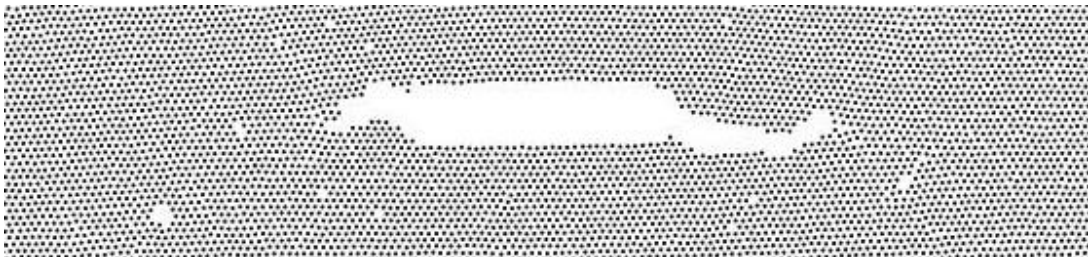


Figure 5: Crack dynamics between 72,000 and 88,000 MCC.

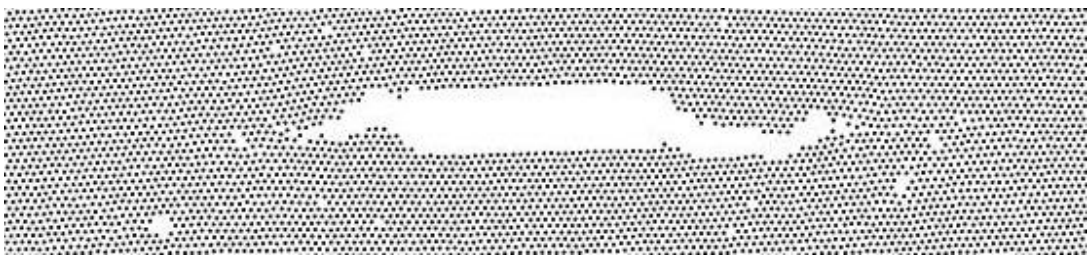
$t = 92000$



$t = 96000$



$t = 100000$



$t = 104000$



$t = 108000$

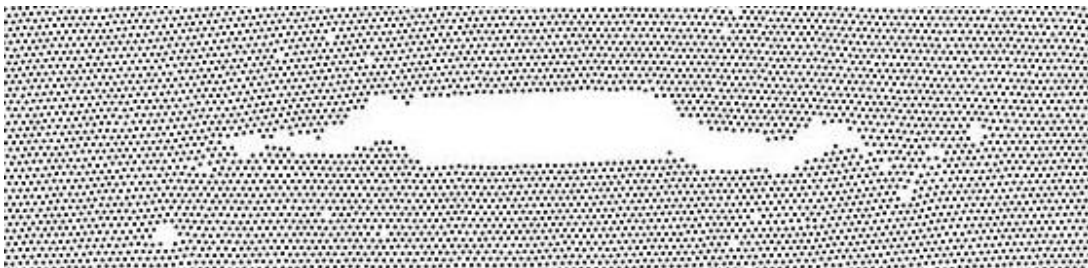
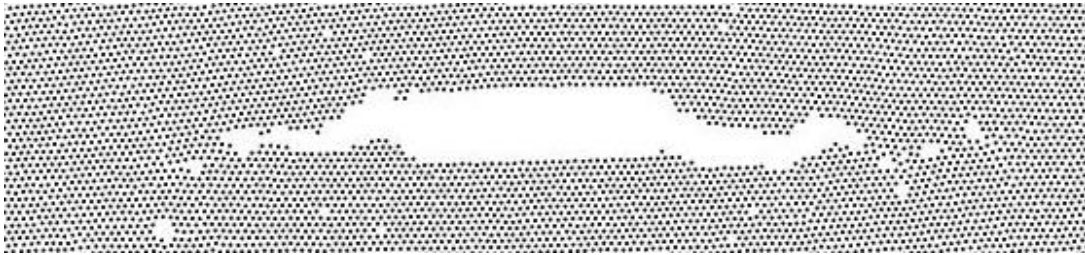


Figure 6: Crack dynamics between 92,000 and 108,000 MCC.

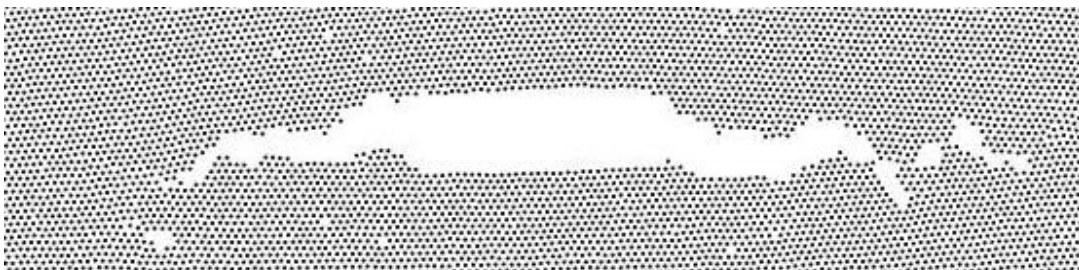
t = 112000



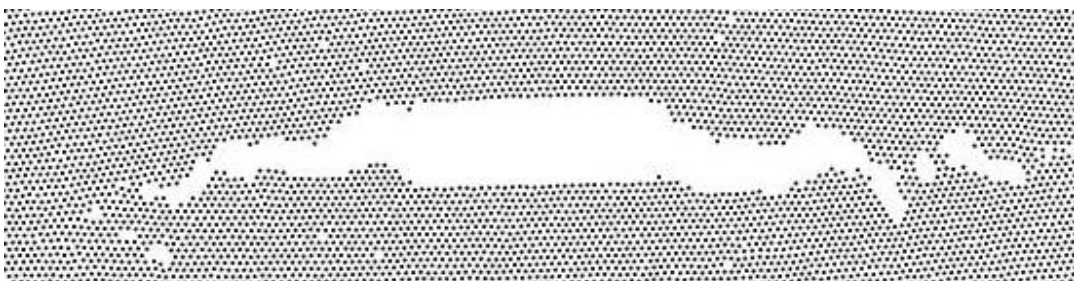
t = 120000



t = 124000



t = 132000



t = 140000



Figure 7: Crack dynamics between 112,000 and 140,000 MCC.

3. Qualitative analytic discussions

Our simulations in Section 2 suggest a theoretical picture of thermally activated crack growth. Such a growth was addressed in the GM conference paper mentioned in the Introduction. The GM discussions were however much too short to exhibit and discuss significant physical and mathematical details (derivations) of the underlying theoretical picture. Therefore, for the first time, we will provide detailed presentation of the theory of thermally activated crack growth. We also stress that new and more extensive simulations described in Section 2 of the present study have provided more advanced insights and some surprising new findings requiring explanation. In the following we will provide analytic theory capable to explain these new findings from our present simulations.

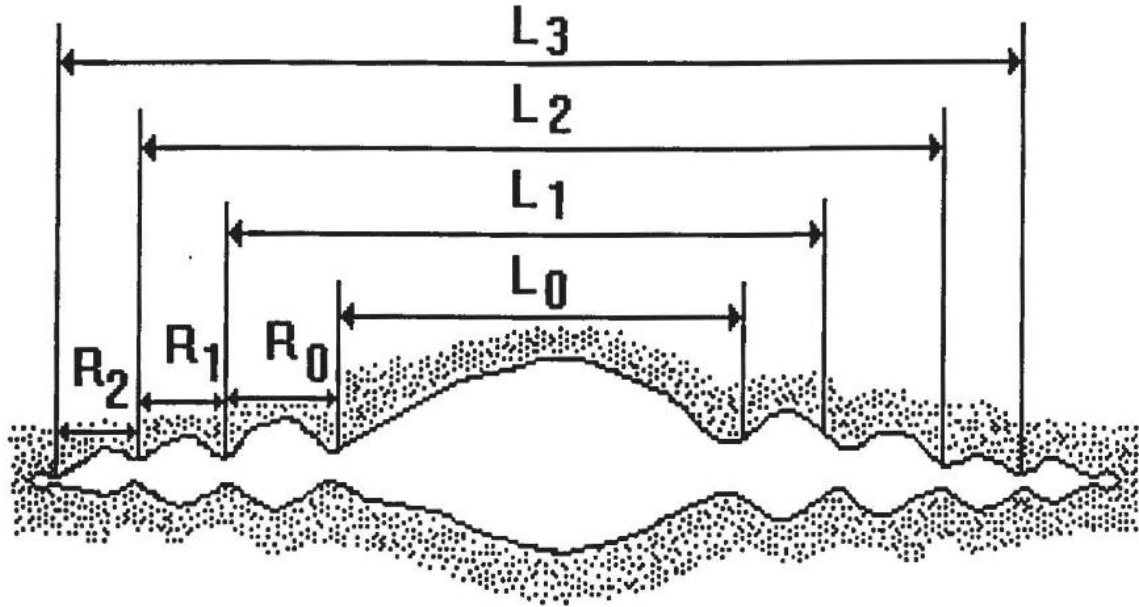


Figure 8: Step-wise character of the thermally assisted crack dynamics.

The crack growth seen in Figures 2 to 7 is stepwise [as summarized in Figure 8]. Each growth step is marked by the formation of one or maybe several cavities nearly of the critical size $R \approx g/\sigma_{loc}$ with energy $\approx E(R) \approx gR$ (see Section 1). Here, σ_{loc} is the stress in the proximity of the rounded crack tip with the rounded tip radius $\approx R$. The tip rounding (blunting) is due to plastic deformations caused by dislocation emissions. The stress $\sigma_{loc} \approx \sigma(\frac{L}{R})^{1/2}$; here, σ is the stress far away from the crack, i.e., externally applied stress. Using these facts, we find,

$$R(L) \approx \frac{R_c^2}{L}, \tag{3}$$

and

$$\sigma_{loc}(L) \approx \frac{L}{R_c} \sigma, \tag{4}$$

where $R_c = g/\sigma$ is the critical cavity size in the *absence* of the crack discussed in Section 1. By Eq. (3), the typical cavity size $R(L)$ substantially depends on the length of the growing crack: For $L = R_c \approx L_{min}$ (the smallest possible crack size introduced by GF; see Section 1), we find $R \approx R_c$ and $\sigma_{loc} \approx \sigma$. On the other end, for $L \approx L_G = gY/\sigma^2$ (the Griffith size crack), we find $R \approx g/Y \approx a$ and $\sigma_{loc} \approx Y \approx \sigma_{max}$. Thus, in agreement with the simulations of Section 2, with growing crack size L , the size of the cavities induced by the

crack, $R(L)$, actually becomes smaller. In fact, the cavity size becomes comparable to the atomic size a when crack size becomes comparable to the Griffith length L_G .

In the limit of weak external stresses σ , the crack growth is composition of many steps (as depicted in Figure 8). The increment of the crack length during each step is comparable with the microcavity size. Thus, the n -th step size,

$$L_{n+1} - L_n = R(L_n) = \frac{R_c^2}{L_n}, \tag{5}$$

decreases with growing crack length. By the difference equation Eq. (5), with $L_{n+1} - L_n \cong \frac{dL_n}{dn}$, one obtains the differential equation,

$$\frac{dL_n}{dn} = \frac{R_c^2}{L_n}. \tag{6}$$

By Eq. (6), $dn = dL_n L_n / R_c^2$ which can be integrated to yield,

$$n = \frac{L_n^2 - L_0^2}{2R_c^2} = \frac{1}{2} \left(\frac{L_n}{R_c}\right)^2 \left[1 - \left(\frac{L_0}{L_n}\right)^2\right]. \tag{7}$$

So,

$$L_n = \sqrt{L_0^2 + 2nR_c^2}, \tag{8}$$

and,

$$L_{n+1} - L_n = R(L_n) = \frac{R_c^2}{\sqrt{L_0^2 + 2nR_c^2}}. \tag{9}$$

By Eq. (7), as the crack length grows from L_0 to L_G , there are

$$n_{max} = \frac{1}{2} \left(\frac{L_G}{R_c}\right)^2 \left[1 - \left(\frac{L_0}{L_G}\right)^2\right], \tag{10}$$

growth steps. Using here the Section 1 relations, $L_G/R_c \approx L_G/L_{min} \approx \sigma_{max}/\sigma$, we get,

$$n_{max} \approx \frac{1}{2} \left(\frac{\sigma_{max}}{\sigma}\right)^2 \left[1 - \left(\frac{L_0}{L_G}\right)^2\right], \tag{10'}$$

(as noted in GM, however without the above detailed derivation) as well as,

$$n_{max} \approx \frac{1}{2} \left(\frac{\sigma_{max}}{\sigma}\right)^2 \left[1 - \left(\frac{\sigma}{\sigma_{max}}\right)^2 \left(\frac{L_0}{L_{min}}\right)^2\right] = \frac{1}{2} \left[\left(\frac{\sigma_{max}}{\sigma}\right)^2 - \left(\frac{L_0}{L_{min}}\right)^2\right] \tag{10''}$$

Note that the number of growth steps n_{max} is generally large for $\sigma \ll \sigma_{max}$.

Because of cavity nucleation, the thermally activated crack growth has prominently stepwise character. Each step is marked by an increase of the crack length by the amount $\Delta L \approx R(L)$. For the n -th growth step, this process takes a time interval proportional to the cavity nucleation time,

$$\Delta t(L_n) \sim \exp\left(\frac{E(R(L_n))}{k_B T}\right) \approx \exp\left(\frac{gR(L_n)}{k_B T}\right) = \exp\left(\frac{gR_c^2}{k_B T L}\right) \tag{11}$$

$R_c = g/\sigma$, so for weak stresses σ , the L -dependence of the step time duration is dominantly due to the exponential term in Eq. (11). By Eq. (11), the step time duration strongly decreases, i.e., the crack growth rate substantially increases as the crack size L increases. This is in agreement with the simulations of Section 2.

The growth time required for a crack starting with the size L_0 to reach L_G , is given by the sum,

$$\tau_{growth} = \sum_{n=0}^{n_{max}} \Delta t(L_n) \cong \int_{n=0}^{n_{max}} dn \Delta t(L_n) .$$

This result can be expressed as,

$$\tau_{growth} \cong \int_{L=L_0}^{L_G} dL \frac{1}{\frac{dL}{dn}} \Delta t(L)$$

Thus, by Eq. (6),

$$\tau_{growth} \cong \int_{L=L_0}^{L_G} dL \frac{L}{R_c^2} \Delta t(L)$$

Therefore, by Eq. (11),

$$\tau_{growth} \sim \int_{L_0}^{L_G} dL \frac{L}{R_c^2} \exp\left(\frac{gR(L)}{k_B T}\right) = \int_{L_0}^{L_G} dL \frac{L}{R_c^2} \exp\left(\frac{gR_c^2}{k_B T L}\right)$$

As $R_c = g/\sigma$, for weak stresses σ the above integral is exponentially dominated by its lower limit, $L \approx L_0$. This yields the crack growth time,

$$\tau_{growth} \sim \exp\left(\frac{gR(L_0)}{k_B T}\right) = \exp\left(\frac{gR_c^2}{k_B T L_0}\right). \tag{12}$$

This result can be expressed in a more informative form by writing the exponent therein as

$$\frac{gR_c^2}{k_B T L_0} \approx \frac{gL_{min}^2}{k_B T L_0} = \frac{gL_{min}}{k_B T} \frac{L_{min}}{L_0} .$$

Above, we employed Section 1 relations,

$$R_c = \frac{g}{\sigma} \approx \frac{aY}{\sigma} = L_{min} .$$

As $Y \approx \sigma_{max}$, we have

$$L_{min}(\sigma) \approx \frac{a\sigma_{max}}{\sigma} .$$

Thus, for the exponent in Eq. (12) we get,

$$\frac{gR_c^2}{k_B T L_0} \approx \frac{gL_{min}^2}{k_B T L_0} = \frac{gL_{min}}{k_B T} \frac{L_{min}}{L_0} \approx \frac{g \frac{a\sigma_{max}}{\sigma}}{k_B T} \frac{L_{min}}{L_0} = \frac{\sigma_{max}}{\sigma} \frac{T_m}{T} \frac{L_{min}(\sigma)}{L_0} .$$

Here,

$$T_m = \frac{ga}{k_B} ,$$

is a temperature scale comparable to the temperature activating breaking of single atomic bonds. By the above results, the crack growth time Eq. (12) can be approximately expressed as

$$\tau_{growth} \approx \exp\left(\frac{\sigma_{max}}{\sigma} \frac{T_m}{T} \frac{L_{min}(\sigma)}{L_0}\right), \tag{12'}$$

as noted in GM, however without providing any of the above detailed derivations. For $L_0 = R_c \approx L_{min}$ (the minimal size cracks introduced by GF), the growth time in Eq. (12) coincides with the result found in GP for the

microcavity nucleation time $\sim \exp\left(\frac{E_{cav}(R_c)}{k_B T}\right) \sim \exp\left(\frac{gR_c}{k_B T}\right)$; see Section 1. On the other end, for the Griffith size cracks with $L_0 = L_G \approx \frac{\sigma_{max}}{\sigma} L_{min}$, the crack nucleated microcavities have the atomic scale size, a , and the crack growth time in Eq. (12') becomes microscopic $\sim \exp\left(\frac{T_m}{T}\right)$. That is, the crack growth time scale becomes comparable to the time needed for thermally activated breaking of single atomic bonds.

A striking finding, notable from our simulations in Figures 2 to 7, is that the crack remains nearly straight during its thermally activated growth. Its transverse deviation, perpendicular to the initial horizontal crack direction, appears to be relatively small. This is rather surprising finding, having in mind a stochastic nature of this growth. To understand this, let us estimate the transverse displacement, W , of the crack tip. After n steps, the crack surface will be a zig-zagged line of n segments. The length of the n -th segment is $\approx R(L_n)$ (the microcavity typical size, Eq.(3)). After n steps, the crack tip exhibits both longitudinal and transverse displacements relative to its initial position: In addition to the tip's longitudinal displacement (perpendicular to the external tensile stress),

$$R(L_0) + R(L_1) + \dots + R(L_{n-1}),$$

the crack tip also displaces in the transverse direction (along the tensile stress), in a random manner, by the distance,

$$W_n = p_0 R(L_0) + p_1 R(L_1) + \dots + p_{n-1} R(L_{n-1}).$$

Here, p_i are uncorrelated random numbers with $\langle p_i \rangle = 0$ and $\langle p_i^2 \rangle \approx 1$. $\langle p_i p_j \rangle \approx 0$, for $i \neq j$, as there are no significant correlations between nucleation events in different steps. Therefore,

$$\langle W_n \rangle = 0,$$

while,

$$\langle W_n^2 \rangle = \langle (\sum_{i=0}^{n-1} p_i R(L_i))^2 \rangle = \langle \sum_{i=0}^{n-1} \sum_{j=0}^{n-1} p_i p_j R(L_i) R(L_j) \rangle.$$

Here, the average is done with respect to the realizations of the random numbers p_i . So,

$$\langle W_n^2 \rangle = \sum_{i=0}^{n-1} \sum_{j=0}^{n-1} \langle p_i p_j \rangle R(L_i) R(L_j).$$

As noted above, $\langle p_i p_j \rangle = \delta_{i,j}$. Thus,

$$\langle W_n^2 \rangle = R^2(L_0) + R^2(L_1) + \dots + R^2(L_{n-1}),$$

or, by Eq. (3),

$$\langle W_n^2 \rangle = \frac{R_c^4}{L_0^2} + \frac{R_c^4}{L_1^2} + \dots + \frac{R_c^4}{L_{n-1}^2} \cong \int_0^n dn' \frac{R_c^4}{L_{n'}^2}.$$

By using this and Eq. (8), we find that,

$$\langle W_n^2 \rangle = \int_0^n dn' \frac{R_c^4}{L_0^2 + 2n'R_c^2}.$$

Calculating the above integral yields the result,

$$\langle W_n^2 \rangle = R_c^2 \ln \left(\frac{\sqrt{L_0^2 + 2nR_c^2}}{L_0} \right). \tag{13}$$

By Eqs. (13) and (8),

$$\langle W_n^2 \rangle = R_c^2 \ln \left(\frac{L_n}{L_0} \right).$$

So, the typical transverse tip displacement W for the crack of the length L behaves as

$$W(L) = R_c \sqrt{\ln \left(\frac{L}{L_0} \right)}. \quad (14)$$

Thus, the deviation of the crack from the straight direction grows only as a square root of the *logarithm* of the crack's length. For all practical purposes, the logarithmic factor in Eq. (14) can be ignored, and W is nearly a constant length $\approx R_c$. Indeed, because L and L_0 are both in the range between L_{min} and L_G , the argument of the logarithm in Eq. (14) is smaller than $\frac{L_G}{L_{min}} = \frac{\sigma_{max}}{\sigma}$. Thus, unless the external stress σ is astronomically small (and the sample astronomically large and old), the logarithmic factor in Eq. (14) can be ignored. Therefore, the theory predicts that cracks remain nearly straight during thermally activated growth. This theoretical finding is in agreement with our simulations of Section 2 in Figures 2 to 7. Strikingly, the simulations indeed show that thermally activated crack growth remains well directed in spite of the random character of the growth process. The zig-zagged path marked by a crack growing from an initial size to the Griffith size L_G is thus significantly less rough than, for example, directed polymers, growing interfaces, or rapidly growing cracks longer than L_G for which W frequently grows as power of the crack length L .

4. Summary and discussion

To summarize, in this study we used numerical simulations to study the nature of the thermally activated dynamics of cracks shorter than the Griffith length in monocrystals. This growth is a sequence of steps each involving a nucleation of a microcavity close to the crack tip, and creation of a passage between the microcavity and the crack. If the external tensile stress σ is much smaller than σ_{max} , many such nucleation events occur before the crack length reaches the Griffith size. As the crack length grows, the size of a nucleated cavity = the increment of crack length during a steps, decreases. Because of this, the energy barrier for the cavity nucleation also decreases with increasing crack length. So, the crack growth rate increases with increasing crack length as documented by our simulations and the theory of Section 3. The crack's transverse roughness W grows very slowly, as the square root of the *logarithm* of crack length. Thus, during the thermally activated crack growth, the crack remains essentially straight, as was indeed observed in the simulations in Figures 2 to 7. This finding is striking since thermally assisted crack growth is essentially a stochastic process.

Our study has investigated these phenomena via an atomistic dynamical simulation which allows having a closer look at what is actually going on in the crack tip region. We thus find that, in monocrystals, an important role in vacancy and cavity nucleation may be played by crack emitted dislocations [Section 2]. For example, we see, in the crack tip vicinity, nucleation of dislocation-vacancy pairs. Such an object dissociates and yields a vacancy and a released dislocation, which may again transform into a dislocation-vacancy pair, etc. Thus, we find an interesting source of vacancies active in the crack tip region. In principle, other mechanisms assisting microcavity nucleation are also possible in monocrystals. For example, the stress gradient should drive thermally (or otherwise) excited vacancies towards crack tips. Agglomeration of these vacancies may nucleate microcavities. However, in a crystalline solid, our simulations indicate that this vacancy-drift scenario is insignificant in comparison to a much faster vacancy production mediated by the crack emitted dislocations. We stress that we found this feature from simulations of a two-dimensional crystal. It remains for future simulations of 3D monocrystals to investigate similar phenomena involving dislocation lines and compare their efficiency with other mechanisms of vacancy and microcavity nucleation. Also, it would be of interest to simulate thermally assisted crack growth in amorphous,

glassy materials. In glasses, standard dislocations are absent! However, some (more restricted) slip-type collective motion can be still envisioned to assist nucleation of microcavities nearby crack tips in a structural glass. Alternatively, a mechanism similar to the vacancy-drift scenario is maybe more typical for glasses. These issues remain to be investigated in future studies.

References

- Brenner, S. S. (1965). Factors influencing the strength of whiskers, *Fiber Composite Materials*. Metals Park, OR: American Society for Metals.
- Edwards, B. C., & Westling, E. A. (2003). *The Space Elevator: A Revolutionary Earth-to-Space Transportation System*. USA: BC Edwards.
- Golubović, L., & Feng, S. (1991). Rate of microcrack nucleation. *Physical Review A*, 43(10), 5223–5227.
- Golubović, L., & Knudsen, S. (2009). Classical and statistical mechanics of celestial-scale spinning strings: Rotating space elevators. *EPL*, 86(3).
- Golubovic, L., & Knudsen, S. (2019). Dynamic Equilibria in Statistical and Nonlinear Physics of Uniform Stress Rotating Space Elevators (USRSE). *Applied Physics Research*, 11(6), 56.
- Golubović, L., & Moldovan, D. (1995). Mechanism of Thermally Assisted Creep Crack Growth. *MRS Proceedings*, 408, 223.
- Golubović, L., & Peredera, A. (1995). Mechanism of time-delayed fractures. *Physical Review E*, 51(4), 2799–2804.
- Golubović, L., Peredera, A., & Golubović, M. (1995). Nature of environmentally assisted fracture nucleation and crack growth in polycrystals. *Physical Review E*, 52(5), 4640–4645.
- Griffith, A. A. (1921). The phenomena of rupture and flow in solids, *Philosophical Transactions of the Royal Society of London Series A* 227, 163. doi:10.1098/rst.0 a.1921006
- Herring, C. (1950). Diffusional viscosity of a polycrystalline solid. *Journal of Applied Physics*, 21(5), 437–445.
- Herring, C. (1950). Effect of change of scale on sintering phenomena. *Journal of Applied Physics*, 21(4), 301–303.
- Knudsen, S., & Golubović, L. (2014). Rotating space elevators: Physics of celestial scale spinning strings. *European Physical Journal Plus*, 129(11).
- Landau, L. D. & Lifshits, E. M. (1970). *Theory of Elasticity*. Oxford: Pergamon.
- Mott, N. F. (1948). Fracture in metals: theoretical considerations. *Engineering* 165, 16.

Copyrights

Copyright for this article is retained by the author(s), with first publication rights granted to the journal.

This is an open-access article distributed under the terms and conditions of the Creative Commons Attribution license (<http://creativecommons.org/licenses/by/4.0/>).